# Computer Simulation of Asymmetric Polymer Mixtures

**M. Müller* and K. Binder**

*Institut für Physik, Johannes Gutenberg Universität, Staudinger Weg 7, D-55099 Mainz, Germany*

*Received July 25, 1994; Revised Manuscript Received December 9, 1994®*

ABSTRACT: In the framework of the 3D bond fluctuation model the phase transition of asymmetric polymer mixtures is studied in the semi-grand-canonical ensemble by a Monte Carlo simulation. The asymmetry is realized by different chain lengths ($N_B/N_A = 2$ or 3) of the two types of polymers. Monomers of the same kind interact via an attractive square well potential extended over the first peak of the pair correlation function, whereas monomers of different types repel each other. We determine the equation of state and discuss the dependence of the critical temperature and density on chain length and asymmetry. The results are related to predictions of the Flory−Huggins theory via the intermolecular pair correlation function of the macromolecular fluid.

## 1. Introduction

Polymer mixtures have attracted increasing interest over the past decade for several reasons:

From the theoretical point of view, the statistical mechanics of these complex fluids pose very exciting problems. The Ginzburg criterion[1] affirms that the behavior of polymer blends becomes mean-field-like in the long chain length limit. Only in the ultimate vicinity of the critical point should one see a critical behavior, corresponding to the 3D Ising universality class. The dependence of the crossover from the mean field to the Ising regime on chain length has been extensively studied in experiments,[2−4] analytic theory,[5,6] and computer simulations,[7,8] finding that there is a rather extended crossover regime and that the mean-field behavior is reached only for very long chain lengths.

Furthermore, computer simulations of asymmetric systems reveal finite size corrections to the order parameter distribution, rooted in the so-called "field-mixing" phenomenon.[9−11] These corrections to scaling are general to asymmetric fluids and have to be taken into account, extrapolating finite size simulation data to the thermodynamic limit.[12] They are also pertinent to the present Monte Carlo study of asymmetric polymer mixtures.

On the other hand, polymer blends are important in material science, because "alloying" polymers potentially results in new materials with improved characteristics. Therefore a detailed knowledge of the microscopic parameters which control the miscibility is indispensable. Despite its great importance, a thorough theoretical understanding of macromolecule miscibility is still missing.

The standard analytical description of the thermodynamic properties of binary polymer mixtures is the Flory−Huggins theory.[13,14] However, this mean-field theory of a simple polymeric lattice model involves drastic approximations (e.g., inappropriate treatment of excluded volume restrictions). Recently, there have been several new theoretical approaches which try to overcome some of the approximations and to incorporate microscopic model features to account at least on a coarse-grained level for chemical details: the integral equation theories of Lipson and co-workers,[15−18] cluster variational methods,[19] the lattice cluster approach of Freed et al.,[6,20] and the P-RISM theory of Schweizer et al.[21−24] The integral equation calculations of Schweizer for structurally symmetric blends using a new molecular closure essentially confirm the results of the Flory−Huggins theory for the critical temperature and $\chi$-parameter, relating the latter to the local structure of the fluid via the intermolecular pair correlation function.

All these approaches neglect composition fluctuations of the mixture, which dominate the behavior in the vicinity of the critical point. Using field theoretical methods, de la Cruz et al.[25] tried to incorporate composition fluctuations, leading to a renormalization of the $\chi$-parameter even in the infinite chain length limit. Recent calculations by Holyst et al.[5] claim, however, that these fluctuation effects vanish with growing chain length. However, they find corrections to the Flory−Huggins critical temperature and critical density for finite chain lengths. Nevertheless, none of the above-mentioned theories can describe the crossover from the mean-field regime to the 3D Ising behavior, which is seen in experiments[2,3] and computer simulations.[7,8]

Comparing analytic theories to experiments often runs into difficulties, because an analytical treatment of the detailed chemical microstructure is not feasible and polymers fulfilling the theoretical idealizations are often not available either. Furthermore, there is only a limited range of chain lengths and temperatures, given by the onset of thermal degradation at high temperatures or the glass transition at low temperatures, accessible to experiments.[26] Therefore conclusive experimental tests of theoretical predictions are very difficult. Only recently has the molecular weight scaling[26] of the critical temperature been experimentally found to be in agreement with the mean-field description.

Of course, the determination of the phase diagram of a chemically realistic model via computer simulation is not feasible, because of the widespread time and length scales of relevance.[27,28] However, computer simulations complement theory and experiment, being well suited to test the various approximations involved in the analytical theories by treating simple coarse-grained models. Earlier Monte Carlo studies of the critical behavior of binary polymer mixtures have focused on the scaling of the critical temperature and amplitudes with chain length[29,30] and investigated the crossover from the Ising to the mean-field regime for symmetrical ($N_A = N_B$) polymer mixtures.[7,8] Furthermore, asym-

® Abstract published in *Advance ACS Abstracts,* February 1, 1995.

0024-9297/95/2228-1825$09.00/0 

metric monomer interactions have been studied,[31-33] where one finds good agreement of the asymmetry dependence of the critical temperature with the predictions of a mean-field treatment.

In the present study, we employ a recently developed algorithm to study mixtures of different chain lengths in the semi-grand-canonical ensemble. We investigate the validity of the mean-field theory and focus our interest on the critical point behavior of these asymmetric polymer blends. The scaling of the critical temperature and critical composition on the chain length asymmetry is studied. Furthermore, the relation of the phenomenological Flory–Huggins parameter $\chi$ to the local structure of the coarse-grained polymer model is investigated.

The outline of the paper is as follows: In section 2 we introduce the model and give a brief summary of the simulation algorithm. Then we discuss the equation of state and its relation to the microscopic structure of the model in section 3. Section 4 starts with a brief review of the data analysis techniques pertinent to asymmetric systems and presents our results concerning the critical point location. Finally, section 5 contains a discussion and an outlook on future work. In an appendix, we give a brief derivation of the mean-field theory for the bond fluctuation model to supply the pertinent analytical description and motivate the definition of model-dependent quantities.

## 2. The Bond Fluctuation Model (BFM) and Computational Details

Since we are interested in the universal thermodynamic features of asymmetric polymer blends, the choice of our polymer model is guided by computational efficiency. Lattice models of polymers have proven to be especially useful in computer simulations. A small number of chemical repeat units (or a Kuhn segment) is mapped onto a lattice monomer such that the relevant features of polymeric systems are retained: connectivity of the monomers along a chain, excluded volume of the monomers, and a short-range thermal interaction. In accord with previous studies, we use the bond fluctuation model (BFM).[34] It has found widespread applications in computer simulation of polymers, because it combines computational tractability of lattice models with a rather good approximation of continuous space features.[34] Furthermore, there exists a variety of information concerning the static,[35] dynamic,[36,37] and thermodynamic properties,[34,38] and "real" polymers can be mapped onto this coarse-grained model.[39] In the framework of the BFM, each monomer occupies a whole unit cell of a simple cubic lattice with periodic boundary conditions. Monomers along a polymer are connected via one of 108 bond vectors of the set $P(2,0,0)$, $P(2,1,0)$, $P(2,1,1)$, $P(2,2,1)$, $P(3,0,0)$, and $P(3,1,0)$, where $P$ denotes all permutations and sign combinations. The large number of possible bonds is particularly important for the employed algorithm. The system comprises a mixture of two species of polymers, which we denote A and B, consisting of $N_A$ or $N_B$ monomers. In the present study we chose $kN_A = N_B$ with $k = 2$ and 3. We work at a filling fraction of $\Phi_\cdot = 0.5$. Due to the extended monomer structure, this density corresponds to a dense polymer melt[35] and the screening length of the excluded volume interactions is roughly given by six lattice constants. Therefore the chain configurations obey Gaussian statistics, $R^2 = c_N\langle l^2\rangle(N-1)$, where $l$ denotes the bond length. Thus the statistical segment length $c_N \approx 1.4$, measured by the number of monomers, is close to its ideal random walk value. We use periodic boundary conditions throughout, and the system size $L$, ranging from 32 to 112, is measured in units of a lattice constant. The presence of vacancies permits local fluctuations of the monomer density, resulting in pronounced packing effects.

Mapping "real" polymers onto the BFM, the monomeric interactions are transformed into effective interactions of the coarse-grained monomers. The thermal interactions between the different species are chosen such that the system exhibits a phase separation upon lowering the temperature. Since we are mainly interested in universal features, the choice of spatial range of the thermal interactions is given by computational convenience. Therefore the inter- and intrachain monomer interactions are modeled by a square well potential extended over the first peak of the pair correlation function, i.e., comprises the 54 neighbor sites up to a distance $\sqrt{6}$.

$$\epsilon = \epsilon_{AB} = -\epsilon_{AA} = -\epsilon_{BB} > 0$$

Monomers of the same kind attract each other, whereas different types exert a repulsion. As discussed below, the specific choice of the thermal interaction potential does not change the qualitative behavior in the long-chain limit.

The Monte Carlo simulation comprises two kinds of Monte Carlo moves, relaxing the polymer configuration and the composition of the mixture:

Semi-grand-canonical steps change the composition of the mixture, leaving the monomer positions unaltered. These Monte Carlo moves consist of joining $k$ A chains at their ends to form one B chain or cutting a B chain into $k$ pieces of equal length. This is illustrated in Figure 1 for $N_A = 3$ and $N_B = 9$. Since the BFM has a favorable ratio of the number of bonds to the monomer volume, it is particularly advantageous for this semi-grand-canonical algorithm, resulting in a sufficiently high acceptance ratio of these kinds of moves. To fulfill the detailed balance condition, the number of possible connection partners of an A-chain end enters in the acceptance probability. A detailed description of the algorithm is given in ref 40.

To relax the chain configurations between the semi-grand-canonical Monte Carlo moves, we use a combination of random local monomer displacements and slithering snake kind of motions. Both the semi-grand-canonical and the slithering snake moves illustrate that completely unphysical moves permit a very efficient relaxation of the configurations in computer simulation. Furthermore, the computation effort is directed to the relaxation of the order parameter (i.e., the composition of the mixture), resulting in smaller relaxation times than in the canonical ensemble.

The ratio between the semi-grand-canonical and canonical moves is adjusted such that the composition fluctuations and the chain configurations relax on the same time scale. For all but the combination $N_A = 40$ and $N_B = 120$ we used local displacements:slithering snake:semi-grand-canonical = 4:12:1, while for $N_A = 40$ and $N_B = 120$ we increased the number of semi-grand-canonical moves by a factor of 4, because of its low acceptance rate.

The free model parameters are the temperature and well depth $\epsilon$ of the thermal interaction and the difference of the chemical potentials of the two monomer types $\Delta\mu = \mu_A - \mu_B$, whereas the composition of the

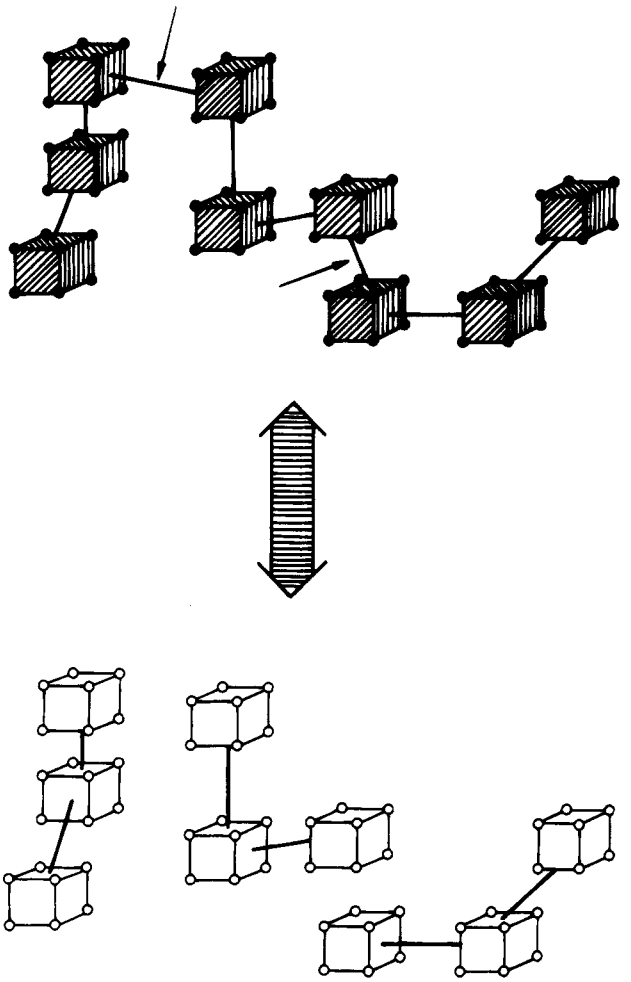

**Figure 1.** Semi-grand-canonical moves for asymmetric polymer mixtures ($k = 3$). Each monomer occupies 8 sites of an elementary cube of a simple cubic lattice. A monomers are shown in white while B monomers are shaded. The bonds that are removed ($N_B \rightarrow 3N_A$) or added ($3N_A \rightarrow N_B$) are indicated by arrows.

mixture is allowed to fluctuate in the semi-grand-canonical ensemble. Since the total number of monomers $\mathcal{N}$ is constant, we describe the composition of the mixture by the reduced density of A monomers.

$$\varrho = \mathcal{N}_A/\mathcal{N}$$

The energy and the composition of the mixture are stored in a histogram and we use Ferrenberg–Swendson techniques[41] to extrapolate to nonsimulated values of the model parameters $\epsilon$ and $\beta\Delta\mu$. This is particularly reliable in the critical region,[42] because the histograms cover a wide range of composition and energy range.

## 3. Equation of State, $\chi$-Parameter, and Local Structure of the Polymeric Fluid

The direct accessibility of the equation of state is another principal advantage of the simulations in the semi-grand-canonical ensemble. This determines the composition of the mixture as a function of temperature and chemical potential difference. Being the derivative of the free energy expression with respect to the composition $\varrho$, the equation of state establishes the direct contact between the simulation data and analytical predictions.

First we turn to the athermal limit. For symmetrical mixtures ($N_A = N_B$)[43–47] the athermal equation of state

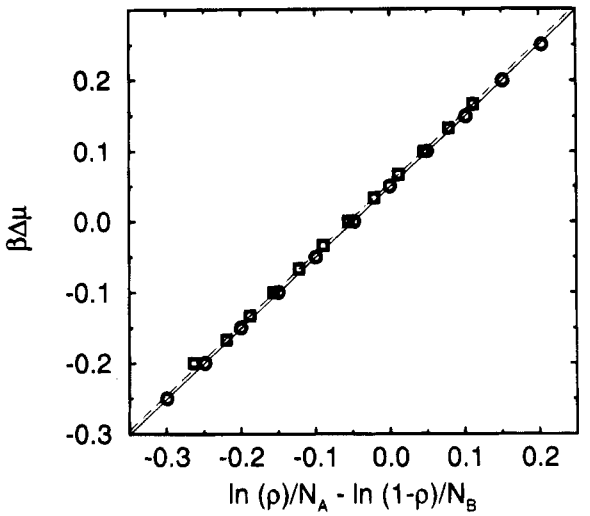


**Figure 2.** Athermal equation of state for chain lengths $N_A = 10$ and $N_B = 20$ (circles) and $N_A = 10$ and $N_B = 30$ (squares). The straight lines correspond to fits according to the mean-field behavior. $N_A = 10, N_B = 20$: $\beta\Delta\mu = (1/N_A)\ln(\varrho) - (1/N_B)\ln(1 - \varrho) + 0.0488$ (solid line). $N_A = 10, N_B = 30$: $\beta\Delta\mu = (1/N_A)\ln(\varrho) - (1/N_B)\ln(1 - \varrho) + 0.0557$ (dashed line).

reduces to a trivial random mixing problem. For asymmetric blends there is an additional contribution due to the entropy density difference of the pure phases. According to the mean-field theory (cf. appendix), this contribution can be approximated by an additional constant $C$ independent of the composition $\varrho$ of the mixture.

$$\beta\Delta\mu = \frac{1}{N_A}\ln(\varrho) - \frac{1}{N_B}\ln(1 - \varrho) - 2\epsilon z_c\{2\varrho - 1\} + C \tag{1}$$

with

$$C = \frac{1}{N_B}\ln\left(\frac{4N_B}{z_B\Phi_{\parallel}}\right) - \frac{1}{N_A}\ln\left(\frac{4N_A}{z_B\Phi_{\parallel}}\right) \tag{2}$$

and $2\epsilon z_c = \chi$. As shown in Figure 2 the chemical potential varies linearly with $(1/N_A)\ln(\varrho) - (1/N_B)\ln(1 - \varrho)$, and the fitted straight lines of unit slope determine the additional asymmetry contribution. The mean-field prediction of the entropy density difference $C = 0.0478(5)$ for $N_A = 10$ and $N_B = 20$ and $C = 0.0541(7)$ for $N_A = 10$ and $N_B = 30$ is in agreement with the simulation data $C = 0.0488(6)$ and $C = 0.0557(10)$ within the error, using the effective number of bonds $z_B = 104(1)$ for athermal chains. Therefore the assumption that $z_B$ is independent of composition and that correlations between the chain ends can be neglected is rather well fulfilled even for these short chains.

Turning to the thermal case, above the critical temperature, the mean-field theory predicts an energetic contribution to the equation of state of the form $2\epsilon z_c \cdot \{2\varrho - 1\}$. Note that this contribution is symmetric around $\varrho = 1/2$ and not around the critical composition $\varrho_c$ of the mixture. To extract this energetic contribution, we study the difference of the chemical potential $\beta\Delta\mu$ and its athermal value. As shown in Figure 3 the composition dependence is in excellent agreement with the mean-field prediction.[48] This mean-field behavior far above the critical temperature was also found for symmetrical mixtures by Sariban and Binder.[44] The slope of this curve is proportional to the $\chi$-parameter. According to the mean-field theory, it is given by the

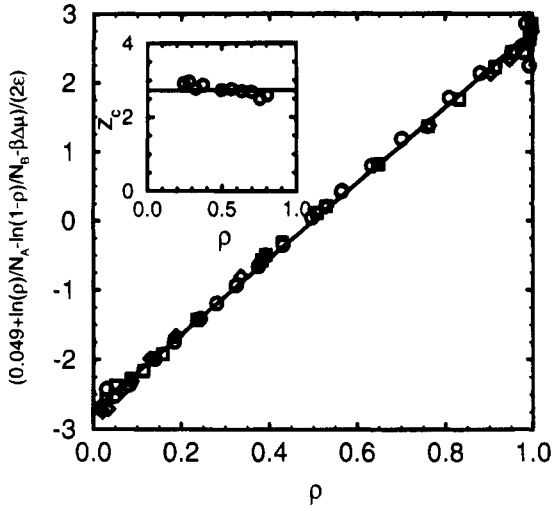


**Figure 3.** $\chi$-parameter and thermal equation of state: difference of the chemical potential ($N_A = 10$, $N_B = 20$) from its athermal value for different temperatures. $\epsilon = 0.01$ (circles), $\epsilon = 0.02$ (squares), $\epsilon = 0.025$ (diamonds). The straight line is given by $(\beta\Delta\mu_{\text{athermal}} - \beta\Delta\mu)/2\epsilon = 2.735(2\varrho - 1)$. The inset shows the determination via the collective structure factor for $\epsilon = 0.01$. The solid line marks the value $z_c = 2.735$.

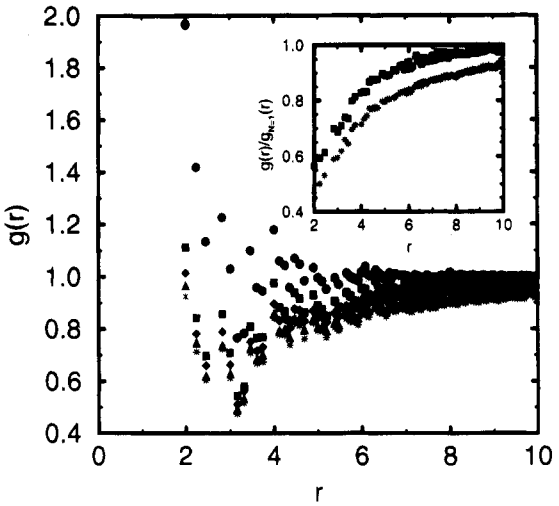


**Figure 4.** Interchain correlation in the athermal limit for different chain lengths: $N = 1$ (circles), $N = 20$ (squares), $N = 40$ (diamonds), $N = 80$ (triangles), and $N = 160$ (stars). The inset shows the correlation function divided by the monomeric equivalent for $N = 20$ and $N = 160$.

coordination number of the thermal *inter*chain potential. This model parameter can be determined by summing the intermolecular pair correlation function $g(r)$ over all 54 sites, belonging to the spatial range of thermal interactions. $g(r)$ is presented in Figure 4 in the athermal limit for a variety of chain lengths. For chain length $N = 20$ in the athermal limit the pair correlation function gives

$$z_c = \frac{\Phi_{|}}{8} \sum_{i=1}^{54} g(\vec{x}_i) = 2.73(2) \tag{3}$$

Note that $g(r)$ is normalized such that $g(r) \to 1$ for $r \to \infty$ and the prefactor in eq 3 accounts for the monomer number density. This value is in good agreement with the value determined by the thermal equation of state. Alternatively, one can resort to the derivative of the equation of state

$$\frac{1}{S_{\text{coll}}(\vec{k}\to 0)} \propto \frac{8}{L^3\Phi_{|}(\langle\varrho^2\rangle - \langle\varrho\rangle^2)} = \frac{1}{N_A\varrho} + \frac{1}{N_B(1-\varrho)} - 4\epsilon z_c \tag{4}$$

to determine $z_c$. This procedure is routinely used in experimental studies to extract the $\chi$-parameter from scattering data, but for computer simulations, it is more demanding than the evaluation via the equation of state. The results for the thermal coordination number $z_c$ are presented in the inset of Figure 3 and agree with the previously determined results.[49] Thus, at least for our coarse-grained structurally symmetric mixtures, a microscopic interpretation of the phenomenlogical $\chi$-parameter is possible. Therefore the macroscopic phase behavior can be related to the local correlations in the macromolecular fluid.

Because of its importance for the phase behavior, we discuss the chain length dependence of the fluid structure in a little more detail. The correlation function mirrors two effects: Due to the extended monomer structure the pair correlation function vanishes for distances $r < 2$. The presence of vacancies[50] introduces local packing effects, which give rise to a highly structured correlation function at short distances. One can identify several neighbor shells, which are characteristic of the monomeric fluid. These packing effects are of course absent in simple lattice models, where a monomeric unit occupies a single lattice site and are less pronounced in the BFM than in continuum models.[50] Its length scale is set by the monomer extension or the bond length.

On the other hand, the extended structure of the macromolecules manifests itself in a reduction of contacts with *other* chains on intermediate length scales. The length of this polymeric correlation hole is given by the radius of gyration $R_g \propto N^{1/2}$. To separate the monomeric local packing effects from the rather universal behavior of the polymeric correlation hole,[51] we divide the correlation function by its monomeric equivalent. This ratio $g_N(r)/g_{N=1}(r)$ is the conditional probability of finding a monomer of a different chain at a distance $r$, if there would be one in the monomer fluid. This is shown in the inset of Figure 4. This ratio seems to be largely independent of the monomeric packing and permits a distinction between the local packing of the fluid and the polymeric correlation hole, even though the corresponding length scales are not well separated for the shorter chains. This reduced correlation function shows the expected polymeric scaling behavior, as presented in Figure 5:

$$\frac{g_N(r)}{g_{N=1}(r)} = 1 - \frac{1}{r} f\left(\frac{r}{N^{1/2}}\right) \tag{5}$$

The deepening of the polymeric correlation hole with increasing chain length results also in a chain length dependence of the effective coordination number $z_c$ of the thermal interactions of the form

$$z_c = z_c^{\infty} + \frac{\text{const}}{N^{1/2}} \tag{6}$$

This is shown in Figure 6. The inset refers to a reduced interaction range used by Deutsch and Binder.[8] A fit of the anticipated behavior gives $z_c = z_c^{54} = 2.10(1) + 2.80(6)/N^{1/2}$ and $z_c^6 = 0.307(4) + 0.48(3)/N^{1/2}$ for the reduced interaction range model (cf. Table 1). For very

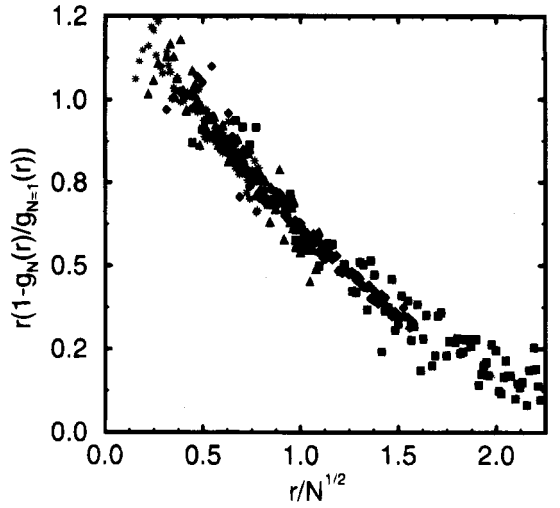


**Figure 5.** Correlation hole effect: scaling of the reduced correlation function $g_N(r)/g_{N=1}(r)$ with chain length (symbols as in Figure 4).

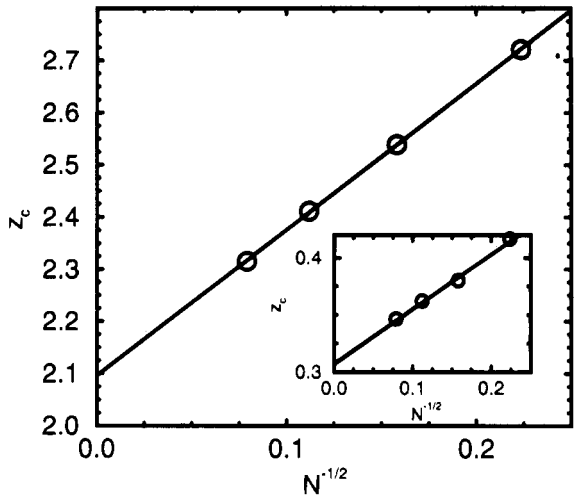


**Figure 6.** Chain length dependence of the thermal coordination number. The inset shows the corresponding behavior for the reduced interaction range.

**Table 1. Effective Coordination Numbers for Two Choices of Interaction Ranges**

| $N$ | $z_c^{54}$ | $z_c^6$ |
|---|---|---|
| 1 | 4.563 | 0.7377 |
| 20 | 2.721 | 0.4166 |
| 40 | 2.539 | 0.3801 |
| 80 | 2.411 | 0.3622 |
| 160 | 2.315 | 0.3462 |

short chain lengths one expects an additional increase of the coordination number due to the effects of the free ends. Furthermore, we only consider athermal systems; a detailed investigation of a possible weak temperature dependence of these structural data is not attempted in the present study. However, these structural data are indispensable for comparing the simulation data to mean-field theories of polymer mixtures, which do not take correlation hole effects into account.

## 4. Scaling Behavior of the Critical Point Location

In the previous section we studied the reliability of the mean-field theory far above the critical temperature and found rather good agreement with our simulation data. However, in the vicinity of the critical point (given by the Ginzburg criterion), the mean-field theory is known to break down for finite chain lengths $N$. Only in the limit $N \to \infty$ are the mean-field results supposed to be recovered.

**Table 2. Critical Temperatures and Densities for All Chain Lengths**

| $N_A$:$N_B$ | $\epsilon_c$ | $N_B\beta\Delta\mu$ | $\varrho_c$ | system size $L$ |
|---|---|---|---|---|
| 10:20 | 0.03196(10) | 0.190(5) | 0.568(5) | 32, 40, 50, 64 |
| 20:40 | 0.01662(5) | −0.492(2) | 0.573(5) | 40, 64, 80 |
| 40:80 | 0.00851(7) | −1.173(1) | 0.578(5) | 64, 80, 112 |
| ∞ | | | 0.586 | |
| 10:30 | 0.02756(15) | 0.1081(5) | 0.610(3) | 32, 40, 50, 64, 80 |
| 20:60 | 0.01426(4) | −1.253(1) | 0.616(5) | 40, 64, 80 |
| 40:120 | 0.00730(5) | −2.618(2) | 0.624(5) | 64, 80, 112 |
| ∞ | | | 0.634 | |

To determine the critical point for asymmetric polymer mixtures in the semi-grand-canonical ensemble, one has to locate the coexistence line and its analytical continuation above the critical temperature in the two-dimensional parameter space of temperature $\epsilon$ and chemical potential difference $\beta\Delta\mu$. In the symmetric case $N_A = N_B$ the coexistence chemical potential difference vanishes; the order parameter distribution and the phase diagram are symmetric around $\varrho_c = 1/2$. Whereas for asymmetric monomer interactions this problem can be solved very elegantly by histogram extrapolation with respect to the asymmetry parameter,[31-33] our algorithm does not permit a continuous variation of the chain length asymmetry. Therefore we resort to the mean-field theory to obtain a first estimate of the coexistence line. Then we use histogram techniques to locate the coexistence line, which is properly defined via the two simultaneous equations

$$\int_0^{\varrho^*} P(\varrho,\epsilon,\beta\Delta\mu_{coex}(\epsilon))\,d\varrho = \int_{\varrho^*}^1 P(\varrho,\epsilon,\beta\Delta\mu_{coex}(\epsilon))\,d\varrho$$

$$\varrho^* = \int_0^1 \varrho P(\varrho,\epsilon,\beta\Delta\mu_{coex}(\epsilon))\,d\varrho \quad (7)$$

where $P$ denotes the probability distribution of the order parameter $\varrho$ at a given temperature $\epsilon$ and chemical potential difference $\beta\Delta\mu$. At a fixed temperature $\epsilon$ below criticality, the coexistence chemical potential $\beta\Delta\mu_{coex}(\epsilon)$ is adjusted such that the two coexisting phases have equal probability. This is illustrated in Figure 7. As discussed thoroughly in ref 12, field mixing effects imply finite size shifts of the form

$$\delta(\varrho_c) \propto L^{-(1-\alpha)/\nu} \quad \text{and} \quad \delta(\beta\Delta\mu_c) \propto L^{-(1-\alpha+\gamma)/\nu} \quad (8)$$

at criticality, whereas this definition is very accurate for the location of the field-driven first-order transition[53] below $T_c$.

Along the so-determined coexistence line, presented in Figure 8, we use the cumulant intersection method to find the critical temperature: Finite size scaling theory[54] implies that the moments of the order parameter $m = \varrho - \langle\varrho\rangle$ can be described in the vicinity of the critical point by

$$\langle|m|^l\rangle = L^{-l\beta/\nu} f_l(L^{1/\nu}(\epsilon - \epsilon_c)) \quad \text{to leading order} \quad (9)$$

Therefore ratios of the form

$$\frac{\langle m^2\rangle}{\langle|m|\rangle^2} \quad \text{and} \quad 1 - \frac{\langle m^4\rangle}{3\langle m^2\rangle^2} \quad (10)$$

become independent of the system size at criticality. Since this method involves only even moments of the

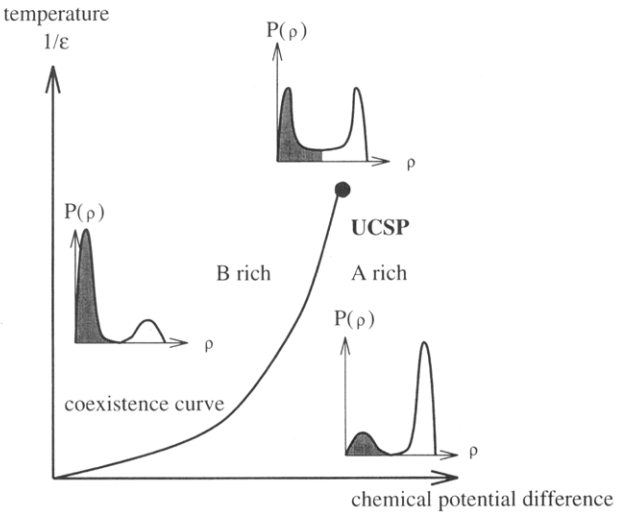


**Figure 7.** Qualitative illustration of the equal-weight criterion. In the semi-grand-canonical ensemble the phase coexistence is given by the line $\beta\Delta\mu_{coex}(\epsilon)$, which ends in the upper critical solution point (UCSP). For $T < T_c$ and $\beta\Delta\mu < \beta\Delta\mu_{coex}$, the system is B-rich and the probability distribution $P(\varrho)$, which is sketched qualitatively in the inset, has a pronounced peak at low composition $\varrho$. This peak is marked by the shaded region. The A-rich peak is however exponentially damped. Right at the phase coexistence, the area under both peaks (shaded and nonshaded) is equal, whereas for $\beta\Delta\mu > \beta\Delta\mu_{coex}$ the A-rich peak dominates and the B-rich one is damped. Between the two peaks, there is a composition region of extremely small probability, which is dominated by properties of the interface between the unmixed phases.

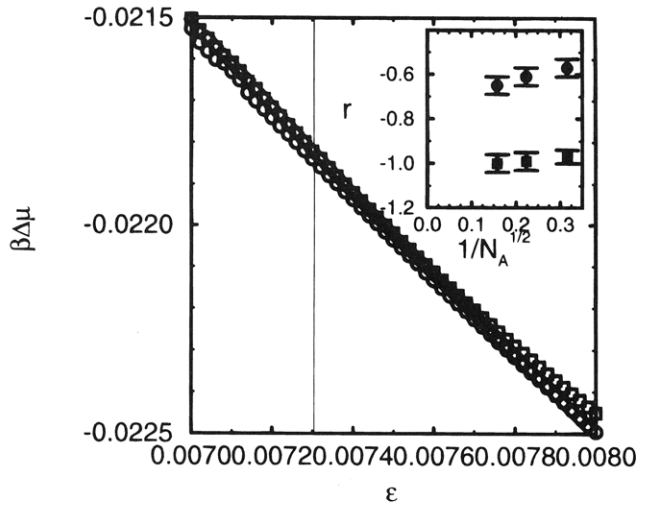


**Figure 8.** Coexistence curve for $N_A = 40$ and $N_B = 120$ using the equal peak weight criterion. $L = 64$ (circles), $L = 80$ (squares), and $L = 112$ (diamonds). The thin line shows the estimated critical interaction parameter. The inset presents the slope of the coexistence line in the vicinity of the critical point, $k = 2$ (circles) and $k = 3$ (squares).

order parameter $m$, it is rather insensitive to asymmetric correction to the order parameter distribution induced by field mixing and small deviations off the coexistence line.[12] This is shown in Figure 9 for the chain lengths $N_A = 40$ and $N_B = 120$. However, note that the universal intersection point of the fourth-order cumulant for such long chains *and* small system sizes does *not* agree exactly with the value of the 3D Ising universality class (as determined in ref 52). This is consistent with the results of Deutsch[8,42] that for small system sizes one observes a broad crossover regime between the mean-field and the 3D Ising behavior,

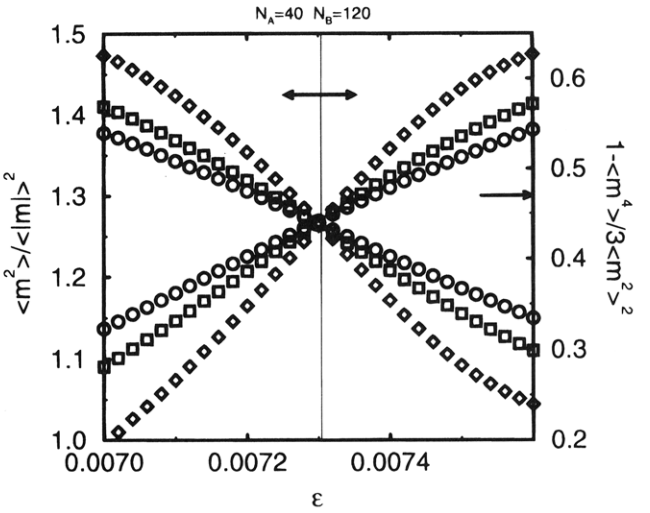


**Figure 9.** Cumulant intersection along the coexistence line ($\langle m^2\rangle/\langle|m|\rangle^2$, falling curves; $\langle m^4\rangle/\langle m^2\rangle^2$, rising curves). From the intersection point for the different system sizes ($L = 64$, circles; $L = 80$, squares; $L = 112$, diamonds), the critical temperature is determined to $\epsilon_c = 0.007304(50)$. The universal value of the fourth-order cumulant for the 3D Ising model is indicated by an arrow on the left side (symbols as in Figure 8).

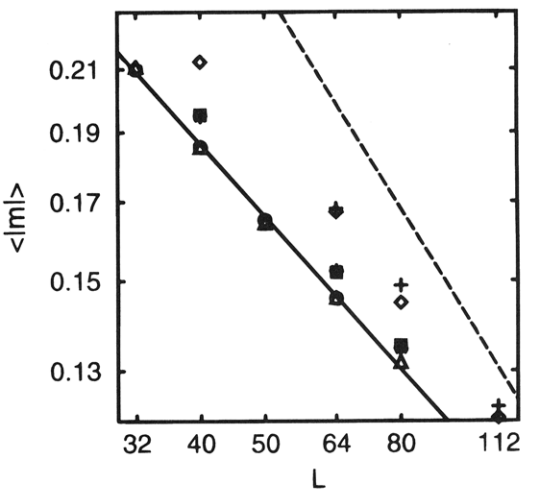


**Figure 10.** Finite size scaling of the order parameter at criticality: $N_A = 10$, $N_B = 20$, circles; $N_A = 20$, $N_B = 40$, squares; $N_A = 40$, $N_B = 80$, diamonds; $N_A = 10$, $N_B = 30$, triangles; $N_A = 20$, $N_B = 60$, stars; $N_A = 40$, $N_B = 120$, pluses. The solid line gives the Ising critical behavior, whereas the dashed line corresponds to mean field predictions.

resulting in *effective* (i.e., system size dependent) critical exponents.[42] For short chain lengths the employed system sizes are large enough to reveal the true critical 3D Ising behavior, whereas one enters the crossover regime from mean field to Ising critical behavior for the longer chains. This is illustrated by the scaling plots for the order parameter (Figure 10) and its susceptibility (Figure 11), where the straight lines correspond to the Ising or the mean-field behavior. Since for our simulation data the ratio $L/N$ is generally larger than in the corresponding studies of symmetric mixtures,[30] the deviations from the Ising critical exponents are rather minor.

The critical temperatures for all chain lengths are plotted in Figure 12 as a function of the "reduced" chain length $N_{red} = 4N_AN_B/(N_A^{1/2} + N_B^{1/2})^2$, suggested by the mean-field theory. The Monte Carlo data for symmetric and asymmetric mixtures collapse onto a single curve, proving that the mean-field theory predicts the chain length dependence of the critical temperature reliably.

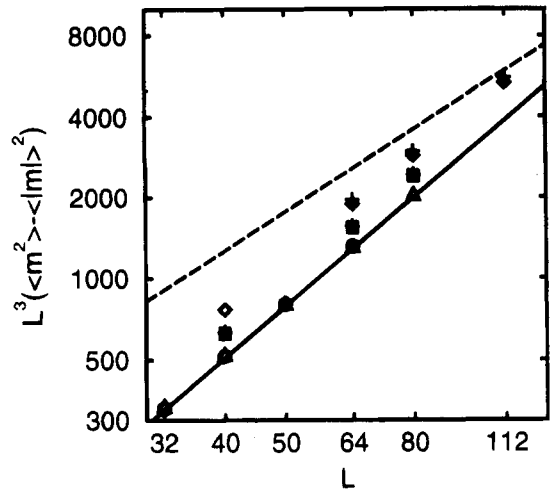


**Figure 11.** Finite size scaling of the susceptibility at criticality (symbols as in Figure 10).

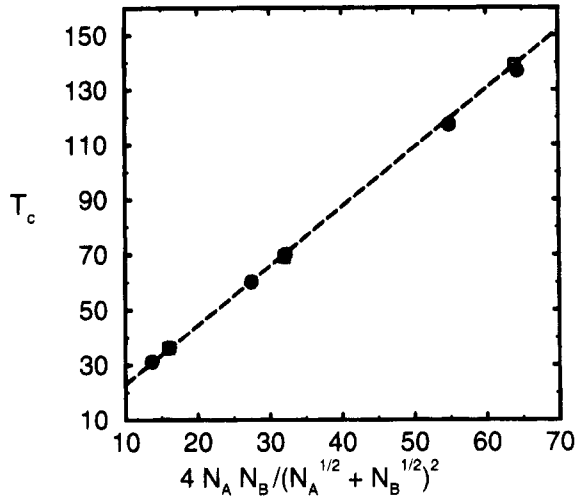


**Figure 12.** Critical temperature vs chain length for symmetric (squares) and asymmetric (circles) mixtures. The dashed line corresponds to $T_c = 2.151N_{red} + 1.35$.

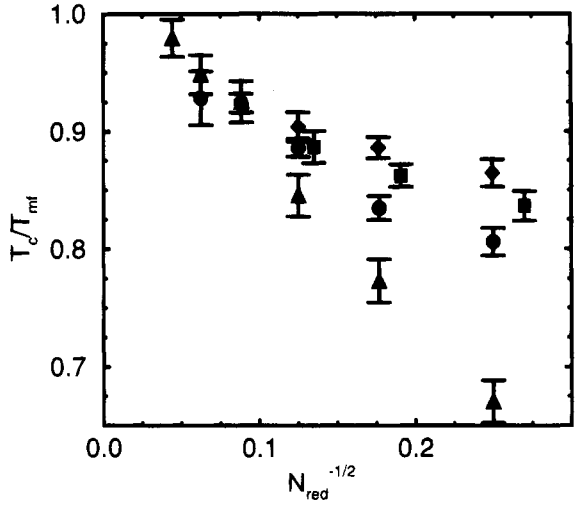


**Figure 13.** Critical temperature divided by the mean-field value: symmetric mixtures (circles); asymmetric mixtures, $k = 2$ (squares) and $k = 3$ (diamonds); symmetric mixtures with reduced interaction range (triangles).

However, for short chains the prefactor is considerably overestimated. This is illustrated in Figure 13, where we draw the ratio $T_c/T_c^{mf}$, using the mean-field critical temperature:

$$T_c^{mf} = z_c \frac{4N_A N_B}{(N_A^{1/2} + N_B^{1/2})^2} \tag{11}$$

For short chain lengths the mean-field theory overestimates the critical temperature about 25%. This is of course not unexpected and a common feature of mean-field theories, due to an inappropriate treatment of critical fluctuations. Reanalyzing the data of Deutsch[8,30] for symmetric mixtures, we find tentative evidence that the relative deviation of the predicted mean-field critical temperature to true critical point vanishes as $1/N^{1/2}$, in accord with the analytical predictions.[5] The data for the asymmetric mixtures show a similar behavior, but they do not collapse onto the corresponding symmetrical set, revealing that $N_{red}$ is not the appropriate scaling combination of $N_A$ and $N_B$, which is not expected. These findings confirm that the shift of the critical temperature from its predicted mean-field value is *larger* than the Ising critical range, given by the Ginzburg criterion.

Next we investigate the critical chemical potential difference $\beta\Delta\mu_c$ on chain length and asymmetry. Its mean-field value is given by

$$\beta\Delta\mu_c = -\frac{1}{N_A}\ln\left(\frac{4e^{1/2}N_A(1 + (N_A/N_B)^{1/2})}{z_B\Phi_{\cdot}}\right) + \frac{1}{N_B}\ln\left(\frac{4e^{1/2}N_B(1 + (N_B/N_A)^{1/2})}{z_B\Phi_{\cdot}}\right) \tag{12}$$

At fixed $k = N_B/N_A$ the critical chemical potential difference is expected to vary as

$$N_B\beta\Delta\mu_c = D + (k - 1)\ln N_A$$

where $D$ denotes a constant independent of $N_A$. This anticipated behavior is presented in Figure 14, where the straight lines correspond to the mean-field prediction using $z_b = 104(1)$. Again the simulation data approach the mean-field values with growing chain length. Even though it is not directly measurable in experiments, this agreement is very important for computer simulations in the grand-canonical ensemble, because it gives a rather reliable prediction of the coexistence line. Therefore it is an invaluable help for choosing a sensitive simulation point in the two-dimensional parameter space of temperature $\epsilon$ and chemical potential difference $\beta\Delta\mu$.

Finally, we consider the dependence of the critical density on asymmetry and chain length. Contrary to the determination of the critical temperature, asymmetric finite size corrections to the limiting order parameter distribution are relevant for an accurate determination of this quantity. Therefore we extrapolate our simulation data according eq 8 to the infinite volume limit. For chain length $N_A = 40$ and $N_B = 120$ such an extrapolation is shown in the inset of Figure 15. Note that the mixed field finite size scaling correction is of the order 2%. For finite chain lengths, the resulting critical compositions are slightly smaller than the mean-field prediction

$$\varrho_c^{mf} = \frac{1}{1 + (N_A/N_B)^{1/2}} \tag{13}$$

However, for growing chain length they approach the Flory–Huggins value from below. This behavior is

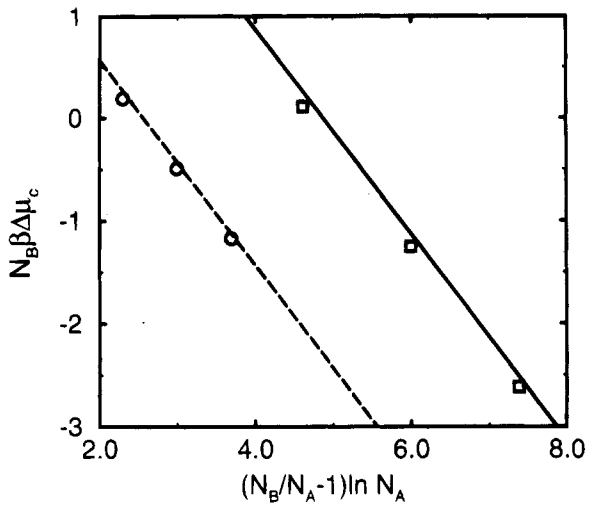


**Figure 14.** Critical chemical potential difference as a function of chain length: $k = 2$ (circles) and $k = 3$ (squares). The straight lines correspond to the mean-field behavior: $k = 2$, $N_B\beta\Delta\mu_c = 2.57 - \ln N_A$; $k = 3$, $N_B\beta\Delta\mu_c = 4.87 - 2 \ln N_A$.

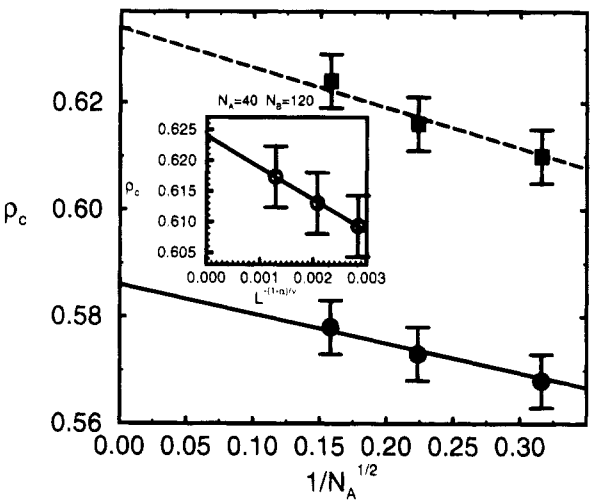


**Figure 15.** Critical composition $\varrho_c$: $k = 2$ (circles) and $k = 3$ (squares). The inset illustrates the extrapolation of the simulation data to the thermodynamic limit according to mixed field finite size scaling for $N_A = 40$ and $N_B = 120$.

presented in Figure 15, where we plot the data vs $1/N^{1/2}$ as suggested by Holyst and Vilgis.[5] As for the deviation for the critical temperature from its mean-field value, our data are consistent with a $1/N^{1/2}$ correction, due to critical fluctuations.

## 5. Summary and Discussion

In the present work, we present a Monte Carlo investigation of the thermodynamics of asymmetric polymer mixtures in the framework of the BFM. The extensive computer simulation uses a recently developed Monte Carlo algorithm[40] for the semi-grand-canonical simulation of mixtures with different chain lengths and comprises a detailed comparison to mean-field theories.

We determine the equation of state both for the athermal system and for temperatures far above the critical point. The simulation data are in agreement with a Flory–Huggins-like description, provided an effective thermal coordination number and an effective number of bonding vectors are used. These effective model parameters can be related to pair correlation functions of the macromolecular fluid.

Using Ferrenberg–Swendsen extrapolation techniques[41] and mixed field finite size scaling,[9,10,12] we locate the coexistence line and the critical point for several chain lengths and two asymmetries $N_B/N_A = 2$ and 3. The critical temperature scales with the reduced chain length $N_{red} = 4N_AN_B/(N_A^{1/2} + N_B^{1/2})^2$, in agreement with the Flory–Huggins theory. This astonishing agreement for all chain lengths is also observed in recent experiments.[55] In the long-chain limit the Flory–Huggins theory becomes an appropriate description; i.e., there is *no* fluctuation-induced renormalization of the $\chi$-parameter as predicted by ref 25. Therefore we are able to relate the microscopic model structure, parametrized by $z_c$ and $z_B$, to the macroscopic phase behavior for structural symmetric blends of different chain lengths. A reexamination of the data of Deutsch et al.[8] for symmetrical mixtures show further that this relation is independent of the spatial range of thermal interactions.

For short chain lengths the critical temperature is overestimated by the mean-field prediction about 25% and our simulation data are consistent with a behavior of the form $(T_c^{mf} - T_c)/T_c \propto 1/N^{1/2}$.

The dependence of the critical composition $\varrho_c$ on chain length asymmetry shows a similar behavior. In agreement with recent calculations of Holyst and Vilgis,[5] the mean-field value is approached from below in the limit $N \to \infty$. This slight overestimation of the critical composition for finite chain lengths is also found in experiments[55] and cluster variational methods.[19]

In accord with the Ginzburg criterion, far above the critical temperature or for very long chains the Flory–Huggins-like predictions become correct. Leading-order fluctuation corrections to the infinite chain length limit have been identified. These are describable by $1/N^{1/2}$ correction terms to the critical temperature and composition. However, in the ultimate vicinity of the critical point 3D Ising critical behavior controls the shape of the coexistence curves, which are illustrated by the scaling behavior of the order parameter at criticality. The consequences of asymmetry at criticality and signatures of field mixing are discussed in depth elsewhere.[12]

The understanding of these asymmetric mixtures is an excellent starting point for investigating the effects of other kinds of asymmetry. Especially structural asymmetries such as different stiffness of the polymer species or different monomer shapes will be a promising topic for future work. It is an interesting question to clarify how such asymmetries influence the composition dependence of the Flory–Huggins parameter at temperatures slightly above criticality, corresponding to the situation of many experiments. In addition, a detailed study of the influence of the thermal interactions on the chain configurations and the fluid structure deserves our attention. Furthermore, these results are fundamental prerequisites for the study of spatially inhomogeneous systems.

**Acknowledgment.** The authors thank N. B. Wilding and W. Paul for helpful discussions. Partial support from the Deutsche Forschungsgemeinschaft (DFG) under Grant No. Bi314/3-2 and a generous grant of CPU time at HLRZ Jülich are also gratefully acknowledged.

## Appendix: Mean-Field Theory

In this appendix, we give a mean-field approximation of a polymer mixture in the framework of the BFM. The derivation is an extension of ref 44 to asymmetric polymer blends. It supplies the pertinent analytical

description, reveals the approximations of the simple mean-field theory, and motivates the definitions of the model parameters $z_c$ and $z_B$.

The starting point for the mean-field approximation is the canonical partition function $\mathcal{Z}$ of a mixture comprising $n_A$ A polymers and $n_B$ B polymers.

$$\mathcal{Z}(n_A,n_B) = \frac{1}{2^{n_A+n_B} n_A! n_B!} \sum_{\{c\}} \exp(-\beta E(\{c\})) \quad (14)$$

where the prefactor takes account of the indistinguishability of chains of the same kind and the head−tail symmetry. $E$ represents the energy of inter- and intrachain potentials. Considering the free energy change in a semi-grand-canonical move $kA \rightleftharpoons N_B$ leads to the Widom-like expression:

$$N_B\beta\Delta\mu = -\ln \mathcal{Z}(n_A+k,n_B-1) + \ln \mathcal{Z}(n_A,n_B) = \ln\left(\frac{2^{k-1}(n_A+k)...(n_A+1)}{n_B}\right) + \frac{\sum_{\{n_A,n_B\}} \exp(-\beta E(\{n_A,n_B\}))}{\sum_{\{n_A+k,n_B-1\}} \exp(-\beta E(\{n_A+k,n_B-1\}))} = \ln\left(\frac{2^{k-1}(n_A+k)...(n_A+1)}{n_B}\right) + \ln\langle\delta_{(\{n_A,n_B\}|\{n_A+k,n_B-1\})} \exp(-\beta(E(\{n_A,n_B\}) - E(\{n_A+k,n_B-1\})))\rangle_{\{n_A+k,n_B-1\}} \quad (15)$$

The average runs over all configurations of distinguishable $n_A + k$ A polymers and $n_B - 1$ B polymers. The $\delta$ expression selects configurations in which $k$ specified A polymers can be connected to a B polymer, whereas the Boltzmann factor accounts for the energy change $\Delta E(kA\rightarrow B)$. Introducing the reduced A-monomer density, one gets in the thermodynamic limit

$$\beta\Delta\mu = \frac{1}{N_A}\ln(\varrho) - \frac{1}{N_B}\ln(1-\varrho) + \frac{1}{N_B}\ln\langle\exp(-\beta\Delta E(kA\rightarrow B))\rangle + \frac{1}{N_B}\ln\frac{(\Phi_1/4)^{k-1}k}{N_A^{k-1}} + \frac{1}{N_B}\ln V^{k-1}p_{k-1} \quad (16)$$

where $p_{k-1}$ denotes the probability for creating a specified B polymer joining $k$ A polymers.

At this point one has to resort to mean-field approximations:

First, in the limit $N \rightarrow \infty$ the spatial correlation between the local environments of the two ends of an A polymer can be neglected and therefore we replace $V^{k-1}p_{k-1}$ by $(Vp_1)^{k-1}$. $p_1$ is the probability that specified ends of two specified A polymers can be connected via one of the 108 bonding vectors of the BFM. As shown in section 3, this is an excellent approximation even for the shortest chains and proves that conformational properties of long chains are very well approximated for $N \geq 10$. Furthermore, the probability $p_1$ is within the range of statistical accuracy independent of the composition of the mixture. Its value can be determined by the pair correlation function $g_{ee}$ of A-polymer ends

$$Vp_{k+1}^{1/(k-1)} \approx Vp_1 = \sum_{i=1}^{108} g_{ee}(\vec{x}_i) := z_B \quad (17)$$

In order to get a rough estimate, one can neglect all local correlations resulting in $z_B \approx 108$. Given the strong local correlations, mainly induced by packing effects, the mean-field approximation turns out to be surprisingly good; nevertheless it is more appropriate to regard $z_B$ as an effective quantity properly defined by the pair correlation function. This gives an effective $z_B = 104(1)$. Furthermore, note that this value may depend weakly on temperature and chain length.

Second, a further approximation concerns the energy change of a semi-grand-canonical move: In the framework of the mean-field theory for the composition fluctuations, its value is given by

$$\beta\Delta E(kA\rightarrow B)) \approx N_B(2\epsilon z_c)\{2\varrho-1\} \quad (18)$$

The validity of this approximation is controlled by the Ginzburg criterion. $z_c$ denotes the effective coordination number of the thermal interchain interactions. Its value can be determined via the interchain monomer pair correlation function $g(x)$:

$$z_c = \frac{\Phi_1}{8}\sum_{i=1}^{54} g(\vec{x}_i) \quad (19)$$

Note that we approximate the AA, AB, and BB interchain correlations by a common correlation function. As pointed out by Schweizer et al.,[22] the differences between these different local correlation functions are supposed to vanish in the limit $N \rightarrow \infty$. In the same spirit, we replace the interchain correlation function by its athermal equivalent. As shown in section 4, this is a rather good approximation in the long-chain limit. Finally, using equations 17 and 18 we arrive at the equation of state (2) as presented in section 2.

In summary, the derivation relies on two types of approximations. One kind, comprising the mean-field approximation for the composition fluctuations and the neglect of the correlation between the local environments of the chain ends, is supposed to become better with growing chain length. The other type concerns the local structure of the polymeric fluid. This is dominated by local packing and correlation hole effects. These approximations, i.e., neglecting spatial correlations on local length scales, are independent of chain length and generally not very accurate. They give rise to the definition of the microscopic nontrivial model parameters $z_B$ and $z_c$, which are properly defined via the corresponding pair correlation functions.

Note further that the entropic contribution is purely combinatorial up to a constant. This feature is related to the structural symmetry of the monomeric units and is *not* expected to hold for structurally asymmetric blends. The additional constant $C$ represents the entropy density difference of the pure phases. Therefore the above equation gives the chemical potential and not only its excess value. Consequently, it is extremely helpful in choosing appropriate simulation points in the two-dimensional parameter space of temperature and chemical potential difference. Using the equation of

state, the critical point is given by the Gibbs criterion:

$$\frac{\partial \beta\Delta\mu}{\partial \varrho} = \frac{\partial^2 \beta\Delta\mu}{\partial \varrho^2} = 0 \tag{20}$$

yielding the well-known results

$$\frac{1}{\epsilon_c} = z_c \frac{4N_A N_B}{(N_A^{1/2} + N_B^{1/2})^2} \tag{21}$$

where $z_c$ is the coordination number of the longer chains

$$\varrho_c = \frac{1}{1 + (N_A/N_B)^{1/2}} \tag{22}$$

$$\beta\Delta\mu_c = -\frac{1}{N_A} \ln\left(\frac{4e^{1/2}N_A(1 + (N_A/N_B)^{1/2})}{z_B\Phi_{\text{I}}}\right) + \frac{1}{N_B} \ln\left(\frac{4e^{1/2}N_B(1 + (N_B/N_A)^{1/2})}{z_B\Phi_{\text{I}}}\right) \tag{23}$$

## References and Notes


(1) Ginzburg, V. L. *Sov. Phys.—Solid State (Engl. Transl.)* **1960**, *1*, 1824. de Gennes, P.-G. *J. Phys. Lett. (Paris)* **1977**, *38*, L-441. Joanny, J. F. *J. Phys.* **1978**, *A11*, L-117. Binder, K. *Phys. Rev.* **1984**, *A29*, 341.
(2) Janssen, S.; Schwahn, D.; Springer, T. *Phys. Rev. Lett.* **1992**, *68*, 3180.
(3) Meier, G.; Momper, B.; Fischer, E. W. *J. Chem. Phys.* **1992**, *97*, 5884.
(4) Schwahn, D.; Meier, G.; Mortensen, K.; Janssen, S. *J. Phys. (Paris) II* **1994**, *4*, 837.
(5) Holyst, P.; Vilgis, T. A. *J. Chem. Phys.* **1993**, *99*, 4835.
(6) Lifschitz, M.; Dudowicz, J.; Freed, K. F. *J. Chem. Phys.* **1994**, *100*, 3957. Dudowicz, J.; Lifschitz, M.; Freed, K. F.; Douglas, J. F. *J. Chem. Phys.* **1993**, *99*, 4804.
(7) Binder, K.; Deutsch, H. P. *Europhys. Lett.* **1992**, *18*, 667.
(8) Deutsch, H. P.; Binder, K. *J. Phys. (Paris) II* **1993**, *3*, 1049.
(9) Bruce, A. D.; Wilding, N. B. *Phys. Rev. Lett.* **1992**, *68*, 193.
(10) Wilding, N. B.; Bruce, A. D. *J. Phys. Condens. Matter* **1992**, *4*, 3087.
(11) Wilding, N. B. *Z. Phys.* **1993**, *B93*, 119.
(12) Müller, M.; Wilding, N. B., to be published in *Phys. Rev. E.*
(13) Flory, P. J. *J. Chem. Phys.* **1941**, *9*, 660.
(14) Huggins, H. L. *J. Chem. Phys.* **1941**, *9*, 440.
(15) Lipson, J. E. G. *Macromolecules* **1991**, *24*, 1334.
(16) Lipson, J. E. G. *J. Chem. Phys.* **1992**, *96*, 1418.
(17) Lipson, J. E. G.; Brazhnik, P. K. *J. Chem. Phys.* **1993**, *98*, 8179.
(18) Sevian, H. M.; Brazhnik, P. K.; Lipson, J. E. G. *J. Chem. Phys.* **1993**, *99*, 4112.
(19) Guevara-Rodriguez, F. J.; Aguilera-Granja, F.; Kikuchi, R. *J. Phys. (Paris) II* **1994**, *4*, 589.
(20) Dudowicz, J.; Freed, K. F.; Lifschitz, M. *J. Chem. Phys.* **1994**, *100*, 3957. Bawendi, M. G.; Freed, K. F. *J. Chem. Phys.* **1988**, *88*, 2741. Pesci, A. I.; Freed, K. F. *J. Chem. Phys.* **1989**, *90*, 2017. Dudowicz, J.; Freed, K. F.; Madden, W. G. *Macromolecules* **1990**, *23*, 4803. Madden, W. G.; Pesci, A. I.; Freed, K. F. *Macromolecules* **1990**, *23*, 1181.
(21) Yethiraj, A.; Schweizer, K. S. *J. Chem. Phys.* **1992**, *97*, 5927.
(22) Schweizer, K. S.; Yethiraj, A. *J. Chem. Phys.* **1993**, *98*, 9053, 9080.
(23) Schweizer, K. S. *Macromolecules* **1993**, *26*, 6033.
(24) Schweizer, K. S. *Macromolecules* **1993**, *26*, 6050.
(25) de la Cruz, M. O.; Edwards, S. F.; Sanchez, I. C. *J. Chem. Phys.* **1988**, *89*, 1704.
(26) Gehlen, M. D.; Rosedale, J. H.; Bates, F. S.; Wignall, G. D.; Almdal, K. *Phys. Rev. Lett.* **1992**, *68*, 2452.
(27) See, e.g.: Binder, K. *Adv. Polym. Sci.* **1994**, *112*, 181.
(28) Binder, K. In *Computational Modeling of Polymers*; Bicerano, J., Ed.; Marcel Dekker: New York, 1992; p 221.
(29) Deutsch, H. P.; Binder, K. *Europhys. Lett.* **1992**, *17*, 697.
(30) Deutsch, H. P.; Binder, K. *Macromolecules* **1992**, *25*, 6214.
(31) Deutsch, H. P. *J. Chem. Phys.* **1993**, *99*, 4825.
(32) Deutsch, H. P.; Binder, K. *Makromol. Chem., Macromol. Symp.* **1993**, *65*, 59.
(33) Deutsch, H. P.; Binder, K. *Polym. Prepr. (Am. Chem. Soc., Div. Polym. Chem.)* **1992**, *33*, 698.
(34) Carmesin, I.; Kremer, K. *Macromolecules* **1988**, *21*, 2819. Wittmann, H. P.; Kremer, K. *Comput. Phys. Commun.* **1990**, *61*, 309. Deutsch, H. P.; Dickman, R. *J. Chem. Phys.* **1990**, *93*, 8983. Deutsch, H. P.; Binder, K. *J. Chem. Phys.* **1991**, *94*, 2294.
(35) Paul, W.; Binder, K.; Heermann, D. W.; Kremer, K. *J. Phys. II* **1991**, *1*, 37.
(36) Paul, W.; Binder, K.; Heermann, D. W.; Kremer, K. *J. Chem. Phys.* **1991**, *95*, 7726.
(37) Baschnagel, J. *Phys. Rev.* **1994**, *B49*, 135.
(38) Müller, M.; Paul, W. *J. Chem. Phys.* **1994**, *100*, 719.
(39) Paul, W.; Pistoor, N. *Macromolecules* **1994**, *27*, 1249. Paul, W.; Binder, K.; Batoulis, J.; Pittel, B.; Sommer, K. H. *Polym. Prepr.* **1992**, *33*, 535; *Makromol. Chem., Macromol. Symp.* **1993**, *65*, 1.
(40) Müller, M.; Binder, K. *Comput. Phys. Commun.* **1994**, *84*, 173.
(41) Ferrenberg, A. M.; Swendsen, R. H. *Phys. Rev. Lett.* **1988**, *61*, 2635; **1989**, *63*, 1195. Bennett, J. *Comput. Phys.* **1979**, *22*, 245.
(42) Deutsch, H. P. *J. Stat. Phys.* **1992**, *67*, 1039.
(43) Sariban, A.; Binder, K. *J. Chem. Phys.* **1987**, *86*, 5859.
(44) Sariban, A.; Binder, K. *Colloid Polym. Sci.* **1988**, *266*, 389.
(45) Binder, K. *Colloid Polym. Sci.* **1988**, *266*, 871.
(46) Sariban, A.; Binder, K. *Colloid Polym. Sci.* **1989**, *267*, 469.
(47) Sariban, A.; Binder, K. *Macromolecules* **1990**, *24*, 578.
(48) These findings are *not* in contradiction to the composition dependence of the $\chi$-parameter of ref 29 on symmetric polymer mixtures, because in the fluctuation-dominated Ising critical region the simple mean-field theory is expected to break down. Estimating the $\chi$-parameter via

$$2N\Phi_{\text{I}}\chi_{\text{eff}} = \frac{1}{\varrho(1-\varrho)} - \frac{4\Phi_{\text{I}}N}{S_{\text{coll}}(\vec{k}=0)}$$

in the ultimate vicinity of the critical point leads to an upward parabolic composition dependence, because the mean-field prediction underestimates the divergency of the collective structure factor $S_{\text{coll}}(\vec{k}=0)$ significantly, resulting in[30]

$$N\Phi_{\text{I}}\chi_{\text{eff}} \approx \frac{1}{2\varrho(1-\varrho)} = \frac{2}{1 - \langle m \rangle^2}$$

where $m$ is defined as in ref 30.
(49) The small negative slope in the data is consistent with a possible chain end effect, discussed in Bawendi, M. G.; Freed, K. F. *J. Chem. Phys.* **1988**, *88*, 2741. They predict a composition-dependent correction term proportional to

$$-\varrho\left(\frac{1}{N_A} - \frac{1}{N_B}\right)$$

for an incompressible melt of self-avoiding walks on a simple cubic lattice.
(50) Yethiraj, A.; Dickman, R. *J. Chem. Phys.* **1992**, *97*, 4468.
(51) de Gennes, P. G. *Scaling Concepts in Polymer Physics*; Cornell University Press: Ithaca (NY) and London, 1979.
(52) Ferrenberg, A. M.; Landau, D. P. *Phys. Rev.* **1991**, *B44*, 5081.
(53) Borgs, C.; Kotecky, R. *J. Stat. Phys.* **1990**, *60*, 79; *Phys. Rev. Lett.* **1992**, *68*, 1734. Borgs, C.; Kotecky, R.; Miracle-Sole, S. *J. Stat. Phys.* **1990**, *62*, 512. Borgs, C.; Kappler, S. *Phys. Rev. Lett.* **1992**, *A171*, 37.
(54) Binder, K. *Z. Phys.* **1981**, *B43*, 119; *Phys. Rev. Lett.* **1981**, *47*, 693. Binder, K. In *Computational Methods in Field Theory*; Gausterer, H., Lang, C. B., Eds.; Springer: Berlin, 1992; p 59.
(55) Budkowski, A.; Steiner, U.; Klein, J.; Schatz, G. *Europhys. Lett.* **1992**, *18*, 705.


MA9412905